Geotech Geol Eng (2024) 42:2271–2291
https://doi.org/10.1007/s10706-023-02637-9

TECHNICAL NOTE

Predicting the Allowable Settlement of Reinforced Soil Foundations: A Laboratory Study

Venkatesh Buragadda · Eswara Reddy Orekanti

Received: 15 December 2022 / Accepted: 2 September 2023 / Published online: 20 September 2023

Abstract It is reported in the literature that the load-carrying capacity of the reinforced sand bed increases with increasing the footing settlement. However, the nature of settlement plays a critical role in shallow foundation designs due to the conditional allowable settlement of the footings. In this present study, laboratory model tests have been performed on a model jute geotextile reinforced sand bed under 1*g* condition. The associated scaling laws are adopted for the geometrical parameters of the model footing and reinforcements as proposed in the literature. On the other hand, a new approach has been developed for the model reinforcements for scaling down of geosynthetic materials under 1*g* condition to simulate the condition of geosynthetic reinforcement layers as in the field or *Ng* conditions. The test results revealed that based on the scaling factors the model footing can be allowed to settle according to the criteria of footing settlement and allowable reinforcement tensile strains. Finally, the suitable guidelines have also been developed as per the safety considerations in order to understand the effect of reinforcement layers on the improvement of soil bearing capacity ratio (BCR) up to a certain settlement ratio (*s/D*) of the footing.

Keywords Reinforced sands · Scaling factors · Model tests · Bearing capacity · Tensile strains · Shallow foundations

V. Buragadda (✉) · E. R. Orekanti
Department of Civil Engineering, School of Engineering, Mohan Babu University (Erstwhile Sree Vidyanikethan Engineering College), Tirupati, Andhra Pradesh 517102, India
e-mail: venkateshiitm15@gmail.com

E. R. Orekanti
e-mail: orekantieswar@gmail.com

1 Introduction

The load-bearing capacity of the foundation can be significantly increased by incorporating the geosynthetic reinforcement layers in different forms such as planar form (i.e., geotextiles, geogrids, and geocomposites), and three-dimensional cellular confinement form (i.e., geocells) into the soil (Lal et al. 2017; Latha and Somwanshi 2009a, 2009b; Shukla et al. 2009; Tafreshi et al. 2016; Chitrachedu and Kolathayar 2020). The mobilized tensile resistance of the reinforcement layers during the loading process fundamentally improves the load-carrying capacity of the reinforced soils (Akbar et al. 2022; Cicek et al. 2015; Ghazavi and Lavasan 2008; Guo et al. 2020). In the case of shallow foundations, several researchers have investigated the effect of different types of planar form of reinforcement layers on the soil load-bearing capacity with respect to the settlement of the footing (Latha and Somwanshi 2009a, 2009b; Cicek et al. 2015; Abu-Farsakh et al. 2013; Aria et al. 2019a, 2021; Basudhar et al. 2007; Binquet and Lee 1975; Buragadda and Thyagaraj 2019; Fragaszy and

Lawton 1984; Ghosh et al. 2005; Kazi et al. 2015; Ouria and Mahmoudi 2018; Shin et al. 2002; Tavangar and Shooshpasha 2016, 2020; Yetimoglu et al. 1994). In the design of shallow foundations, the settlement criteria are the primary factors rather than the bearing capacity criteria (Buragadda and Thyagaraj 2019; Tafreshi and Dawson 2010). However, as per the literature, no constant parameter of footing settlement ratio (represented by *s/D*) has been considered to understand the effect of the reinforcement layers towards improving the soil load-bearing capacity. Notably, (Binquet and Lee 1975) and (Fragaszy and Lawton 1984) have demonstrated the effect of reinforcement layers towards improving the load-bearing capacity of the sand bed in terms of bearing capacity ratio (BCR) up to 10% settlement ratio (*s/D*) of the footing. Abu-Farsakh et al. (Abu-Farsakh et al. 2013) and (Shin et al. 2002) have reported the BCR for the footing settlement (*s/D*) of less than 5% and some of the researchers showed the BCR up to ultimate i.e., 3 to 7% (Yetimoglu et al. 1994; Adams and Collin 1997; Hsieh and Mao 2005; Demir et al. 2013; Guido et al. 1986; Fayaz and Shah 2023).

Few researchers have investigated the effect of reinforcements up to a footing settlement (*s/D*) of 10 to 15% (Latha and Somwanshi 2009a; Tafreshi et al. 2016; Aria et al. 2019a; Buragadda and Thyagaraj 2019; Ouria and Mahmoudi 2018; Tavangar and Shooshpasha 2016, 2020; Tafreshi and Dawson 2010; Demir et al. 2014). Moreover, some researchers have largely demonstrated the BCR at a footing settlement of more than 20% (Lal et al. 2017; Latha and Somwanshi 2009b; Cicek et al. 2015; Aria et al. 2021; Ghosh et al. 2005; Kazi et al. 2015; Akhil et al. 2019; Dash et al. 2004; Patra et al. 2005). Overall, these prior works has demonstrated that researchers considered no any constant parameter of footing settlement ratio (represented by *s/D*) while understand the effect of the reinforcement layers towards improving the soil load-bearing capacity. As per the safety considerations, the footing should be allowed up to a certain footing settlements.

Chenari and Bathurst (2023a, 2023b) performed numerical analysis and investigated the effect of reinforcement tensile properties (i.e., strength and stiffness) on the footing load-bearing capacity under three different soil medium conditions. These studies showcased the reinforcements tensile stiffness (i.e., 500 kN/m to 2000 kN/m) effect on the footing load-bearing capacity by considering various states of footing settlements i.e., serviceability to ultimate limit states. In these studies, the mobilized tensile stiffness of the reinforcements is determined using empirical methods by assuming mobilized stiffness as an equivalent linear stiffness. The test observations revealed that the influence of tensile stiffness on the footing load carrying capacity improvement varies with respective footing settlements. However, irrespective of footing settlements, it judged that the influence of reinforcement stiffness does not show any significance on the load carrying capacity. The scope of these studies is limited to analytical and stochastic finite difference method (FDM) numerical models.

Hence, the current study attempts to determine the mobilization of reinforcement tensile stiffness during footing settlements and its influence on the enhancement of footing load-carrying capacity. In this present study, laboratory model tests have been performed on a model jute geotextile reinforced sand bed under $1g$ condition by considering a new approach while scaling down for the model reinforcements ($1g$) to simulate the condition of geosynthetic reinforcement layers as in the field or Ng conditions. The main highlight of this present study is that the mobilized stiffness of the reinforcements at different footing settlements are determined using pre-calibrated strain gauges. Finally, formulate the guidelines for understanding the effect of reinforcement layers in improving the soil load-carrying capacity up to a certain settlement ratio (*s/D*) of the footing.

1.1 Adopted Scaling Factors for Model Studies

Due to the dominative effect of self-weight forces of the soil, the laboratory model tests under $1g$ condition might not replicate the real behavior of soil as in the field in real-time. To simulate the real behavior of the soil used in the field, the scaling factors should be applied for the model tests. Several researchers have carried out small-scale and large-scale experimental centrifuge model studies on unreinforced and reinforced soils using a smaller size of the footings under different gravity (Ng) conditions (Kusakabe et al. 1992; Cocjin et al. 2013; Liu et al. 2007; Mahmud and Zimmie 1997; Toyosawa et al. 2013; Viswanadham and Konig 2004). A few studies were carried out on scale down geosynthetic (e.g., geotextile and geogrid) reinforced sand beds under normal gravity (1*g*) conditions (Tafreshi et al. 2016; Buragadda and Thyagaraj 2019; Dhanya et al. 2019). The small-scale model tests may represent the footing behavior and general mechanism as occurred in the field (Tafreshi et al. 2016; Cicek et al. 2015; Akhil et al. 2019). Therefore, the model tests are carried out carefully in the present study by considering the scaling factors into account as described here below.

1.2 Modeling of Soil Particles

To simulate the model test results as carried out in the laboratory under 1*g* and *Ng* conditions, the scaling laws should also be applied for the size of soil particles with a scaling factor of *N* (Liu et al. 2007; Pinto and Cousens 1999). However, several researchers have different views with respect to considerations of scaling of the size of soil particles. Some researchers have mentioned that the size of the soil particles should be maintained during model tests as same as the prototype to prevent the different stress–strain behavior with smaller (i.e., model) size of soil particles (Kusakabe 1993; Okamura et al. 2004). In contrast, the soil particle size effect should be considered during the conditions of formation of shear bands and also for the case of considerations of smaller footing size in comparison to the size of soil particles (Okamura et al. 2004; Tatsuoka et al. 1997). The recent study carried out by (Toyosawa et al. 2013) shows that the influence of particle size is negligible on increasing the footing size. However, the influence is not significant even for the smaller footings at lower footing settlement levels. Finally, they proposed a guideline for the consideration of the influence of particle size during the model tests based on the ratio of medium size of soil particles (d_{50}) with the footing size (D) for different embedment depths i.e., the influence of particle size is negligible for the following conditions of $D/d_{50} > 50$ for surface footings and $D/d_{50} > 33$ for embedded footings.

1.3 Modeling of Foundation Material

According to (Wood 2004), the soil stresses and settlements under 1*g* condition should be maintained in the laboratory model as same as in the field apart from the geometrical similarity of the footing. Accordingly, to simulate the same conditions of the soil in laboratory model tests, the flexural rigidity of model footing scaled with the soil stiffness. To simulate the prototype concrete circular footing with Young's modulus of 25 GPa and having dimensions of 1.5 m diameter and 0.25 m thickness, the scaling laws were adopted as proposed by (Wood 2004). As per the findings with scaling down factor of 4, the model footings of 150 mm diameter (D) and 25 mm thick rigid steel plate with a Young's modulus of 200 GPa represented the desired prototype footing. Table 1 summarizes the scaling factors for the foundation material adopted in this present study.

1.4 Modeling of Reinforcement Material

In the case of reinforced sand beds, the allowable tensile strains of the reinforcement layers were found to be up to 2 to 10% (Latha and Somwanshi 2009a, 2009b; Tafreshi et al. 2016; Cicek et al. 2015; Abu-Farsakh et al. 2013; Tafreshi and Dawson 2010; Adams and Collin 1997; Akhil et al. 2019; Dash et al. 2004; Patra et al. 2005; Dhanya et al. 2019; Aria et al. 2019b). To perform the experimental model studies on the reinforced sand beds, the model geosynthetic reinforcement materials exhibiting less tensile strength for the defined strain limit were considered as reported by (Viswanadham and Konig 2004). In order to simulate the natural properties of prototype reinforcement material, the model geosynthetic reinforcement material should satisfy the requirements of tensile stress–strain behavior of an ideal material as shown in Fig. 1. It represents that the model

Table 1 Scaling factors adopted for the present model tests

Parameter	Scaling factor (*N*)(Model/Prototype)
Footing properties	
Size (D)	$\frac{1}{N}$
Footing displacement	$\left(\frac{1}{N}\right)^{1.5}$
Geotextile properties	
Length (L) x width (B_r) x thickness (t_c)	$\frac{1}{N}$
Tensile strength (Tg)	1
Tensile strain (Eg)	$\frac{1}{N^{0.5}}$
Secant modulus (Jg)	$N^{0.5}$
Soil-Geotextile interface properties (Φ_{int})	1

reinforcement should have the tensile strength *(Tg)*$_m$ and secant modulus *(Jg)*$_m$ is $1/N^2$ (for 1*g* model tests) or $1/N$ (for *Ng* model tests) times lesser in comparison with the prototype reinforcement tensile strength *(Tg)*$_p$ and secant modulus *(Jg)*$_p$ for the defined strain limit i.e., $(Eg)_m = (Eg)_p$ (Viswanadham and Konig 2004). As per the authors test observations; interestingly, in most of the practical cases, the commercially available model geotextile reinforcement material exhibits the properties within the allowable tensile strain limits (i.e., < 3–4%) as shown in Figs. 2 (a-b). It can be observed from the lesser reinforcement tensile deformations that the model reinforcement material exhibits either the same (Fig. 2a) or higher tensile strength and stiffness (Fig. 2b) in comparison with the prototype reinforcements. This shows that the model reinforcements do not satisfy the idealized stress–strain behavior at lesser tensile strains as presented in Fig. 1. This is consistent with the model reinforcement test results as reported by Pinto and Cousens (Pinto and Cousens 1999). Hence, an attempt has been made in this present study by considering a different way approach for an idealized tensile stress–strain behavior of the model reinforcement material as presented in Fig. 3, which shows that the model reinforcement material exhibits the same tensile strength *(Tg)*$_m$ as prototype reinforcement *(Tg)*$_p$ at different tensile strains *(Eg)*. However, the model reinforcement material exhibits higher tensile

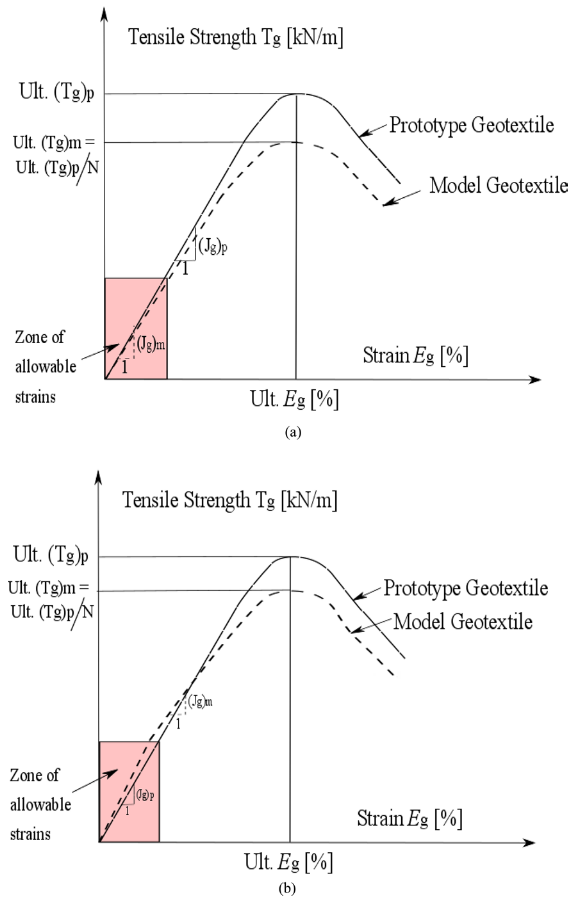

Fig. 2 Different stress–strain behavior of model and prototype geotextile reinforcement at N_g scale model tests: **a** $(Tg)_m = (Tg)_p$ and $(Jg)_m = (Jg)_p$, **b** $(Tg)_m > (Tg)_p$ and $(Jg)_m > (Jg)_p$

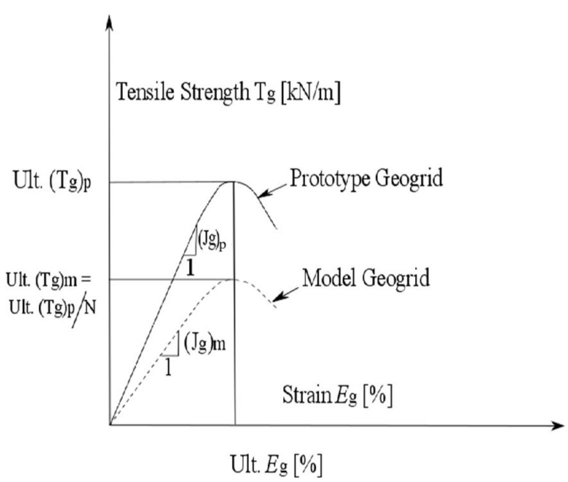

Fig. 1 Idealized stress–strain behavior at *Ng* scale model tests (after Viswanadham and Konig 2004)

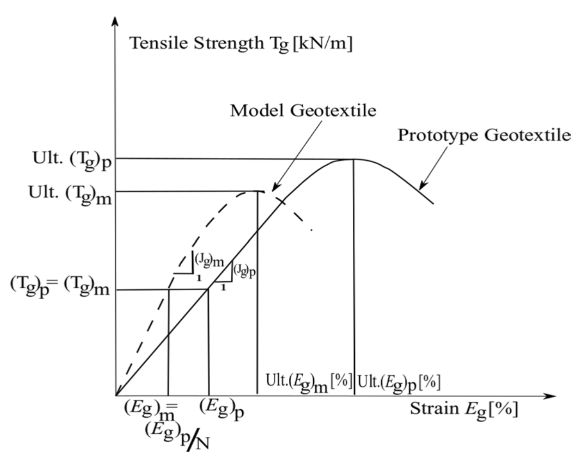

Fig. 3 Idealized stress–strain behavior of model and prototype geotextile

stiffness or secant tensile modulus $(Jg)_m$ as compared to the prototype material $(Jg)_p$. Furthermore, to simulate the proper bond stress between soil-geosynthetic interfaces, the tensile stiffness of the model reinforcement should be higher than the prototype reinforcement (Viswanadham and Konig 2004). In general, natural reinforcement materials such as jute and coir exhibit higher tensile stiffness at lesser tensile strains as compared to synthetic reinforcement materials (Sarsby 2007). Accordingly, in this study, the natural jute geotextile reinforcement material was considered as a model reinforcement material to simulate the real effect of the synthetic geotextile reinforcement layers as used in the real-time field at an allowable strain of 2%.The scaling factors adopted for the reinforcement materials are depicted in Table 1. Moreover, Table 2 listed both model and prototype properties based on scaling factors adopted for the present model tests.

1.5 Laboratory Test Material Properties

1.5.1 Sand

The laboratory model tests were conducted using clean and dry sand collected from Chennai, India. The particle size distribution of the sand is shown in Fig. 4. According to ASTM D6913-17 (ASTM D 6913–17 2017) and as per the Unified Soil Classification System (USCS), the obtained soil was classified as poorly graded sand with a symbol of 'SP'. As per the ASTM D4254-16 (ASTM D 4254–16 2016), the maximum and minimum dry unit weight of the sand was determined to be 17.93 and 15.78 kN/m^3, respectively. In the laboratory model tests, the relative density (R_d) of the sand was maintained as 70%. The angle of internal friction and cohesion of sand was determined at 70% relative density (R_d) from standard small size (60 mm x 60 mm x 25 mm) direct shear test and found to be 39.11° and 0 kPa, respectively. Overall test sand properties have used in the present study is summarized in Table 3. From Table 3, the ratio of model footing size (D = 150 mm) to the medium size of test sand (D_{50} = 0.72 mm) is more than 200. It is almost four times higher than the limit for consideration of negligible particle size influence on load-settlement characteristics of model tests (Toyosawa et al. 2013). Hence, the model tests with soil particle sizes of the present study may replicate the real behavior of the soil as in the field conditions.

1.6 Reinforcement Material

The natural jute geotextile was used as a model reinforcement material in the present study. The jute geotextile was procured from the M/s. Ballyfabs International Ltd., Chennai, India, which is a company approved by the National Jute Board (NJB), Govt. of India. The tensile stress–strain behavior of the jute geotextile was determined from the standard wide-width tension test in each direction as per the ASTM D4595-17 (ASTM D 4595–17 2017), and the obtained tensile stress–strain plots are presented in Fig. 5. Table 4 presents the properties of the reinforcement material used in the present study. From Table 4, it could be said that the secant modulus at 5% strain larger than the corresponding value at 1% strain. Due to high stiffness properties of natural jute geotextile, the tensile stiffness may shows higher at 5% strain in comparison to the strain value of 1%. Moreover, the same effect could

Table 2 Model and prototype properties based on scaling factors adopted for the present model tests

Parameter	Properties	
	Model (1*g*)	Prototype
Footing properties		
Size, D (mm)	150	1500
Footing displacement (mm)	6.25	50
Geotextile properties		
Length (L) x width (B_r) x thickness (t_c) in mm	525 × 525 × 1	2100 × 2100 × 4
Tensile strength, Tg, (kN/m)	0.50	0.50
Tensile strain, Eg (%)	1%	2%
Secant modulus, Jg (kN/m)	50	25
Soil-Geotextile interface properties, Φ_{int} (deg)	28.01^0	28.01^0

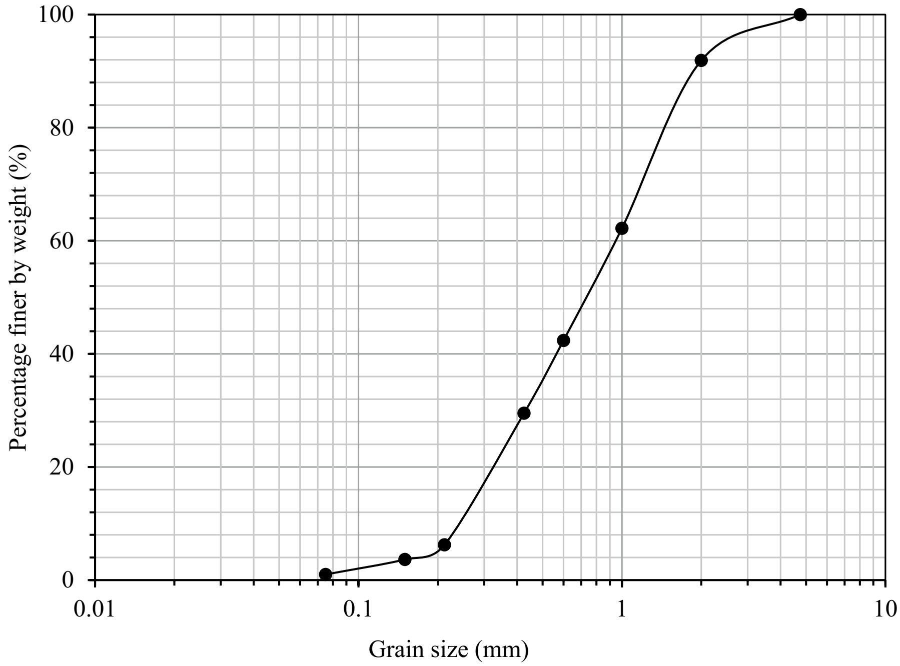

Fig. 4 Grain size distribution curve of sand

Table 3 Properties of sand used in the investigation

Properties	Value
Specific gravity, G_s	2.68
Grain size distribution (%)	
Gravel	0
Sand	99
Fines	1
D_{10} (mm)	0.25
D_{30} (mm)	0.42
D_{50} (mm)	0.72
D_{60} (mm)	0.95
Uniformity coefficient, C_u	3.80
Curvature coefficient, C_c	0.74
Unified soil classification symbol (USCS)	SP
Maximum dry unit weight (kN/m^3)	17.93
Minimum dry unit weight (kN/m^3)	15.78
Dry unit weight corresponding to 70% relative density (kN/m^3)	17.23
Shear strength parameters at 70% relative density:	
Angle of internal friction (°)	39.11
Cohesion (kPa)	0

be observed for the cases of synthetic geotextile and geogrid reinforcements from the literature study of Cicek et al. (Cicek et al. 2015). The sand-geotextile interface properties were determined using a standard small size direct shear test apparatus as per the ASTM D5321–17 (ASTM D 5321–17 2017). The interface properties such as interface friction angle and adhesion were found to be 28.01° and 6.85 kPa, respectively.

1.7 Footing and Test Tank

The model tests were conducted in the present study using a model footing having a size of 150 mm diameter (represented by *D*) and 25 mm thickness. The soil-to-soil interaction (i.e., roughness) at the footing base is incorporated by gluing a thin uniform layer of sand particles using an adhesive material. The load tests were carried out in a steel tank having an inner dimension of 900 mm × 900 mm × 900 mm. The sand bed was prepared up to a depth of 800 mm. To eliminate the side boundaries of the test tank on the soil load-settlement characteristics while performing the model plate load tests, the test tank size was maintained as 6*D* (Buragadda and Thyagaraj 2019). Figure 6a shows the schematic view of the total test set-up used in the present model tests.

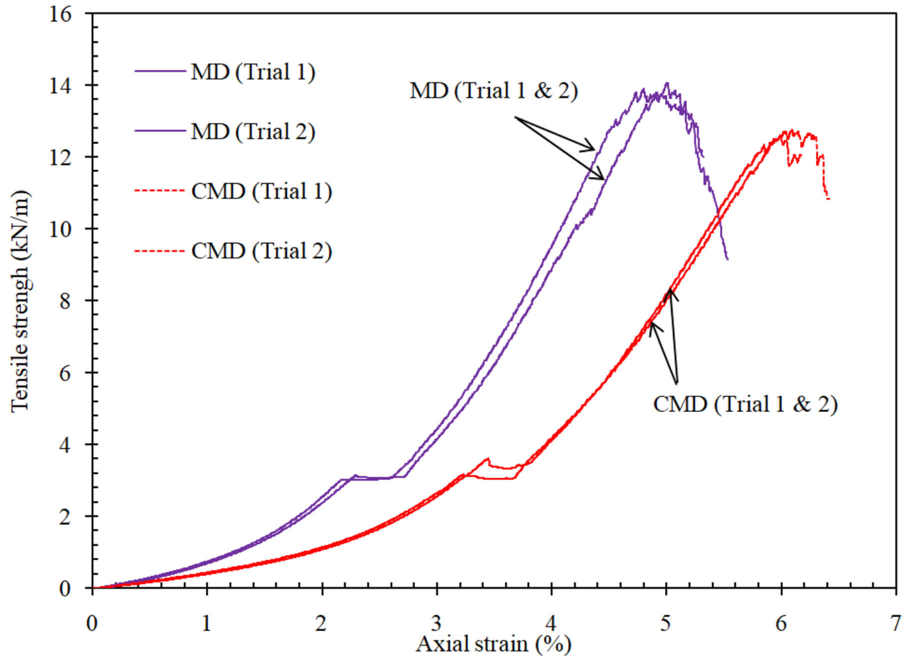

Fig. 5 Tensile strength-strain behavior of model jute geotextile

Table 4 Properties of jute geotextile

Properties of jute geotextile	Standards	Value
Physical properties		
Thickness (mm)	ASTM D5199-12 (ASTM D 5199–12 2012)	1
Mass per unit area (g/m^2)	ASTM D5261-18(ASTM D 5261–10 2018)	315
Mechanical property		
Ultimate tensile strength (kN/m)	ASTM D4595-17 (ASTM D 4595–17 2017)	
MD[a]		13.8
CMD[b]		12.5
Elongation at failure (%)		4.9
MD[a]		5.9
CMD[b]		
Secant modulus at 1% strain, *Jg* (kN/m)		50
Secant modulus at 5% strain, *Jg* (kN/m)		246
Punching strength from CBR plunger test (N)	ASTM D6241-14 (ASTM D 6241–14 2014)	1240
Interface properties	ASTM D5321-21 (ASTM D 5321–17 2017)	
Interface friction angle (°)		28.01
Adhesion (kPa)		6.85

[a]MD stands for machine direction

[b]CMD stands for cross-machine direction

Fig. 6 Laboratory model total test set-up: **a** schematic view **b** photographic view

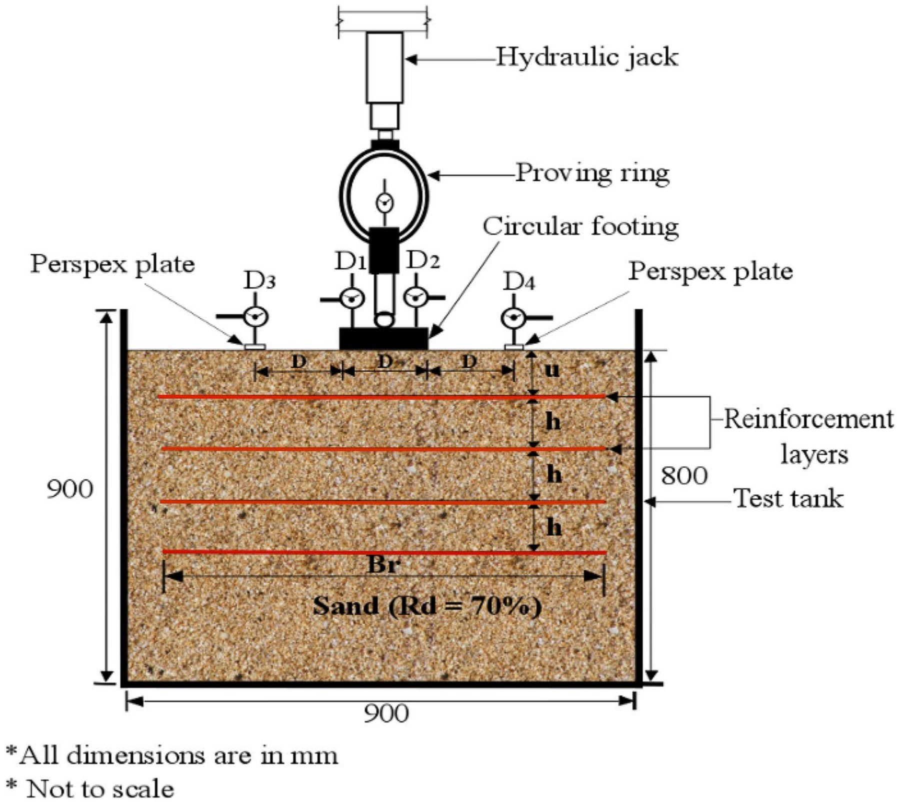

(a)

(b)

1.8 Laboratory Model Tests

1.8.1 Preparation of Sand Bed for Model Tests

The laboratory model tests were conducted on the sand beds prepared by air-pluviation technique. Initially, a series of trials were performed in a model tank having a size of 450 mm × 450 mm × 350 mm with different heights of falls to achieve the desired relative density i.e., 70%. Upon achieving the desired relative density, the corresponding height of fall was maintained the same during the preparation of the sand bed in the test tank (i.e., 900 mm × 900 mm × 900 mm).The relative density of sand was monitored at every 10 cm depth up to a depth of 800 mm during the preparation of the sand bed by placing the known volume of small aluminum cups (5 numbers) at different locations in the test tank i.e., one at the center and four at corners (Latha and Somwanshi 2009a, 2009b; Buragadda and Thyagaraj 2019). The laboratory model tests were conducted on a sand relative density of 70% (i.e., with a dry unit weight of 17.23 kN/m^3).

1.9 Layout of Reinforcement Layers

As aforementioned, the natural jute geotextile was used in the present laboratory model tests. A schematic diagram of the layout of multi-layered geotextile reinforced sand bed adopted in the present study is shown in Fig. 6a, where the indicated terms such as the placement depth of the first reinforcement layer from the footing base (represented by u), the vertical spacing between the reinforcement layers (represented by h), number of layers of reinforcement (represented by N), and the width of reinforcement (represented by B_r) are the geometrical parameters. The reinforcement materials placed at optimum conditions result higher load-carrying capacity (Ghazavi and Lavasan 2008; Guo et al. 2020). Based on the earlier findings of Buragadda and Thyagaraj (Buragadda and Thyagaraj 2019), the optimum geometrical parameters of $\frac{u}{D}$= 0.31, $\frac{h}{D}$= 0.3, N = 4, and $\frac{B_r}{D}$= 3.5 have been used in the present study, and these parameters are reported by Buragadda and Thyagaraj (Buragadda and Thyagaraj 2019) corresponding to the same properties of jute geotextile reinforcement as used in the present study. Moreover, findings of optimum geometrical parameters of the present study are in disagreement with the literature due to the difference in the foundation material properties and reinforcement material properties (Guo et al. 2020; Abu-Farsakh et al. 2013).

1.10 Experimental Procedure

As discussed in the previous sections, the sand bed was prepared in the test tank using the air-pluviation technique. In the case of model tests on reinforced sand beds, the geotextile layers were required to be placed at the desired depths during the preparation of the sand bed. Therefore, the sand was continuously poured inside the test tank until it reaches the placement depth of the geotextile layer. Once it is reached desired depth, the pluviation process was stopped and the soil surface was leveled and confirmed with the spirit level. Thereafter, the geotextile reinforcement layer was placed exactly at the specified depth, then, revamp the pluviation technique upto sand reaches the depth of the placement of next geotextile reinforcement layer. This process was continued until the sand level reaches the desired depth, i.e., 800 mm. In order to avoid eccentric loading, the footing was placed exactly at the center of the hydraulic jack. A circular groove was made exactly at the center of the footing plate to accommodate the ball bearing. A hand-operated hydraulic jack was used to apply the loading onto the footing. The ball bearing arrangement favors the transfer of applied loads uniformly on to the footing in the sand bed. According to IS 1888–1982 (IS 1888), the vertical loads were applied incrementally using a pre-calibrated proving-ring and the load increment was maintained constant until the settlement of footing reached stable i.e., $<$ 0.02 mm/min. As shown in Fig. 6a, the footing settlements were measured with dial gauges of D_1 and D_2 having capacity each can move up to 50 mm run with an accuracy of 0.01 mm. Additionally, the sand surface deformations were measured using dial gauges of D_3 and D_4 having capacity each can move up to 10 mm run with an accuracy of 0.01 mm. Figure 6b illustrates the photographic view of the total test set-up used in the laboratory model tests.

The tensile strains can be developed in the reinforcement layers during the loading on the reinforced sand bed. Accordingly, the mobilized tensile strains were measured by mounting the pre-calibrated electrical resistance strain gauges on the top surface of the reinforcement layers along the vertical direction of the sand

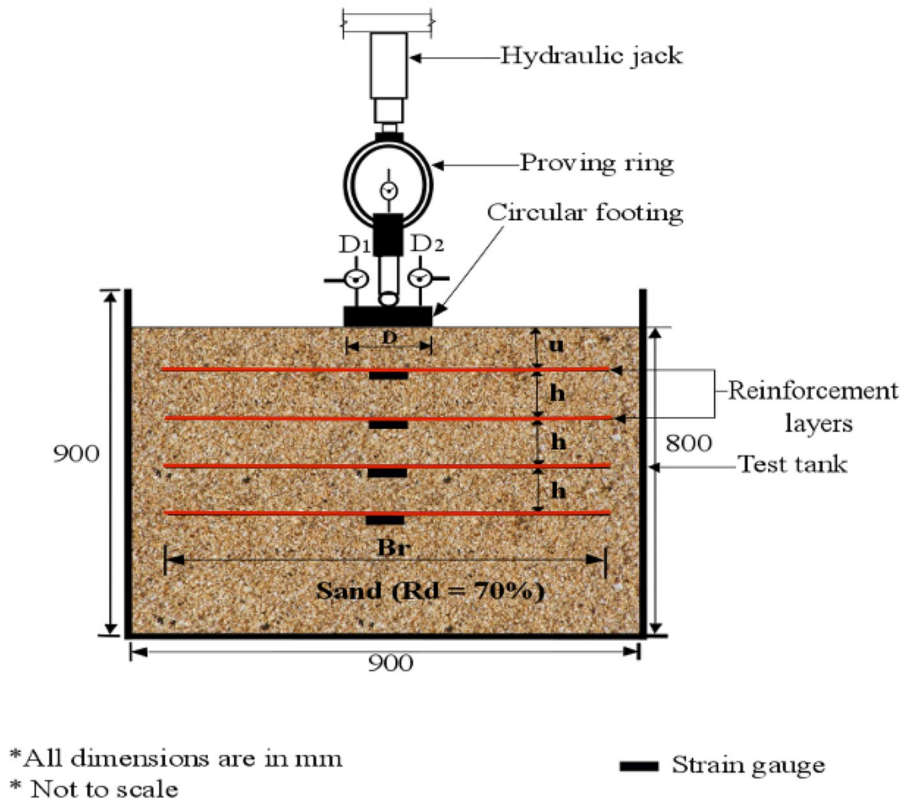

Fig. 7 Schematic representation of model test geometry for multi-layered reinforced sand bed along with strain gauge attachments

bed as shown in Fig. 7. Non-reusable strain gauges were procured from the M/s. TML international Ltd., Chennai, India. The strain gauges are 10 mm in length with a gauge factor of $2.12 \pm 1\%$ and a gauge resistance of $120 \pm 0.2\Omega$. The mobilized tensile strains in the geotextile during loading were determined using a 10-channel Master data logger (Quantum-X, HBM International Ltd.) and for monitoring the readings the data logger was connected to the computer. The model tests of unreinforced and reinforced sand beds were conducted thrice to ensure the consistency of test results. The test findings only indicated a variance of 7%, regardless of the soil test condition. Finally, the average of the three tests is presented as a final result of the current research study.

2 Results and Discussion

2.1 Pre-calibration of Strain Gauges

Initially, a total 5 number of procured TML strain gauges were attached on the surface of jute geotextile reinforcement having a size of 200 mm $\times$ 100 mm is equal to the sample size (gauge) of wide-width tension test as shown in Fig. 8a-b. Figure 8a illustrates that the total geotextile sample was divided exactly into two halves in both horizontal and vertical directions and three strain gauges were attached along the centerline of the vertical axis of the geotextile, i.e., each at the edge and center, and two strain gauges were attached at each edge of the

Fig. 8 Strain gauge locations on the geotextile: **a** schematic view **b** photographic view

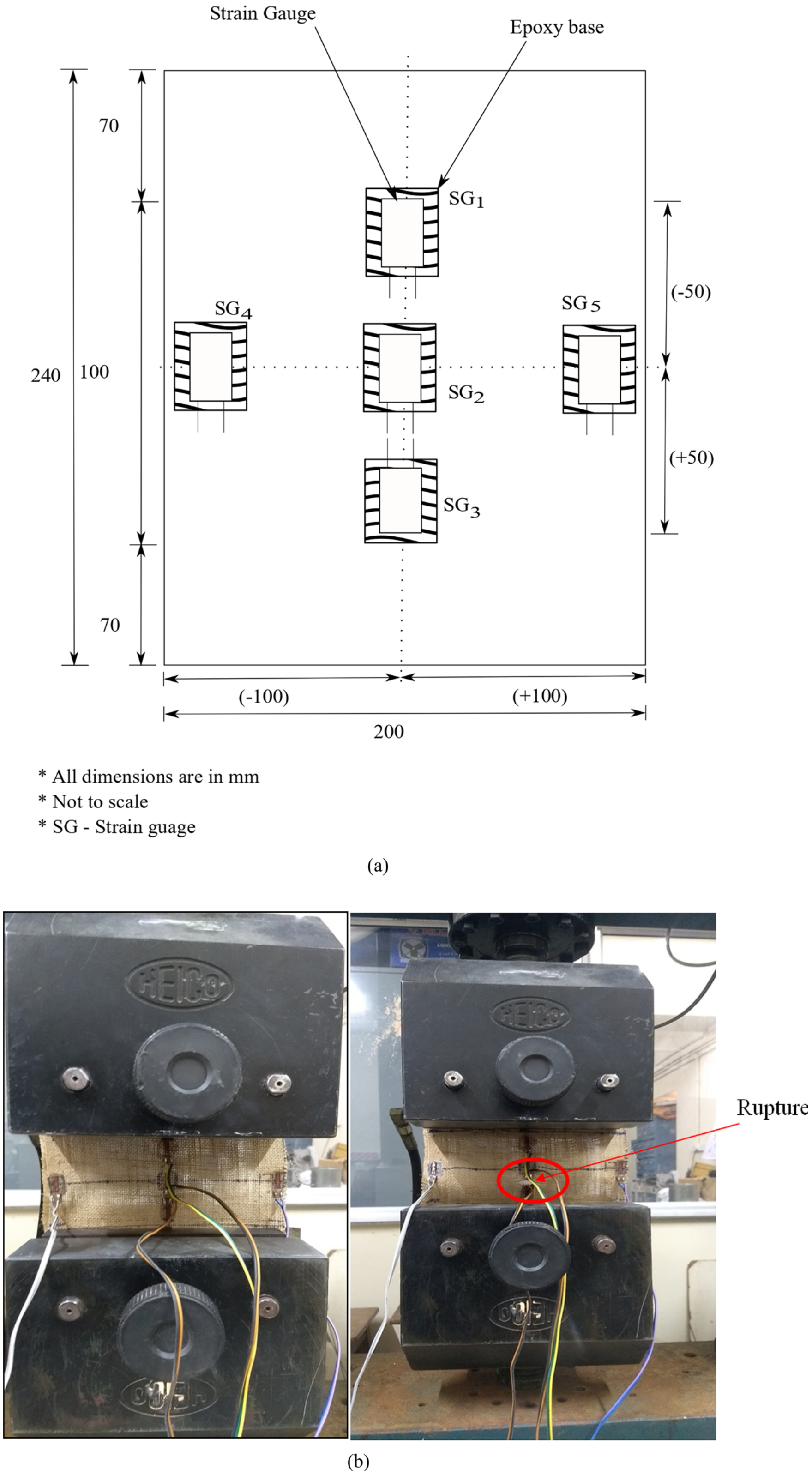

horizontal axis of geotextile. The strain gauges were glued along the horizontal and vertical direction of the geotextile sample by spreading a thin layer (i.e., approximately 20 mm × 15 mm × 1.5 mm) of the uniform mix of Cyanoacrylate adhesive along with epoxy base material only at strain gauge locations. Adequate care should be taken while spreading an adhesive at strain gauge locations to prevent the additional stiffening of the geotextile material with an adhesive as much as possible (Viswanadham and Konig 2004). The lead wires were soldered with the strain gauges and attached to the strain gauge indicator. As per the procedure followed by (Viswanadham and Konig 2004), the strain gauges were pre-calibrated through a load-controlled method by applying a cyclic loading, i.e., loading and unloading using a standard flat hydraulic grip wide-width tensile test apparatus as shown in Fig. 8b. Due to the lower tensile strength property of jute geotextile (i.e., < 50 kN/m), flat hydraulic jacks were used in the present study (Kutay et al. 2006; Skochdopole et al. 2000) rather than roller grips as used by (Viswanadham and Konig 2004). Initially, the strain gauges attached-geotextile samples were fixed into the flat grips of wide-width tension test apparatus and allowed up to a tensile load of 1.35 kN/m (i.e., 10% of ultimate tensile strength), with a strain rate of 10 mm/min. Thereafter, unloaded to zero with the same strain rate. Due to the necessity of stabilization of strain gauge response, initially, two loading–unloading cycles were allowed by maintaining a waiting period of 10 min. Hereafter, the measured tensile strains of the geotextile along the vertical direction and horizontal direction during 3rd and 4th cyclic loadings in two different patterns are shown in Fig. 9a(i & ii) and Fig. 9b(i & ii). To reduce the mess up of strain test results, the variation of strain (average of 3rd and 4th cyclic loadings) at different positions of strain gauges shows upto the tensile load of 0.25 kN/m in Fig. 9a(ii) and 9b(ii). Finally, Figs. 9a(i) and 9b(i) revealed that where the attached strain gauges showed the almost same amount of identical tensile strain responses during two loading cycles, except with different slopes. This is consistent with the strain gauge data reported by (Viswanadham and Konig 2004) .

2.2 Strain Distribution Along the Reinforcement

2.2.1 *During Wide-Width Tensile Test*

Figure 10 presents the average mobilized tensile strains in the reinforcement corresponding to the data obtained from the edges and central position of the strain gauges during the wide-width tensile test of jute geotextile (Fig. 9a-b). It can be observed from Fig. 10 that the mobilized tensile strains in the reinforcement layer increase with increasing tensile loading up to 2.6 kN/m. Notably, at higher tensile loadings, the strain gauges (i.e., central portion strain gauge) are failed.

2.3 Strain Distribution in Reinforcement Layers During Model Tests

As aforementioned, the model plate load tests were conducted on unreinforced and reinforced sand beds using jute geotextile reinforcement layers. The mobilized tensile strains in the reinforcement layers were determined using strain gauges by attaching a similar procedure as followed during pre-calibration tests of strain gauges were conducted on the jute geotextile (Fig. 7). Figure 11 shows the photographic views of jute geotextiles along with attached strain gauges before placing them into the test sand bed. Additionally, small size thin Teflon foil strip was pasted to the jute geotextile (i.e., at the strain gauge locations) with a fine coating of the adhesive material to cover the attached strain gauges, in order to protect against soil particle movements for the elimination of the early failure during testing. Figure 12 shows the variation of load-settlement characteristics of both unreinforced and reinforced sand beds. The variation of Bearing Capacity Ratio (BCR) for different footing settlement ratios (represented by *s/D*) is presented in Fig. 13. BCR is defined as the ratio of reinforced soil bearing pressure to the unreinforced soil bearing pressure at the same settlements. At higher footing settlements (i.e., settlement more than the unreinforced soil peak bearing capacity), the unreinforced soil ultimate bearing capacity is considered during further calculations. From Fig. 12, it could be said that the load-settlement curves of unreinforced sand bed show a peak behavior due to the dense nature of soil sudden failure occurs during loading. Contrastingly, the reinforced soil also shows a peak behavior due to the rupture of

Fig. 9 **a** Calibration curves of strain gauges along horizontal direction of the jute geotextile during cyclic loading: **(i)** upto failure **(ii)** upto 0.25 kN/m **b** Calibration curves of strain gauges along vertical direction of the jute geotextile during cyclic loading: **(i)** upto strain guage failure **(ii)** upto 0.25kN/m

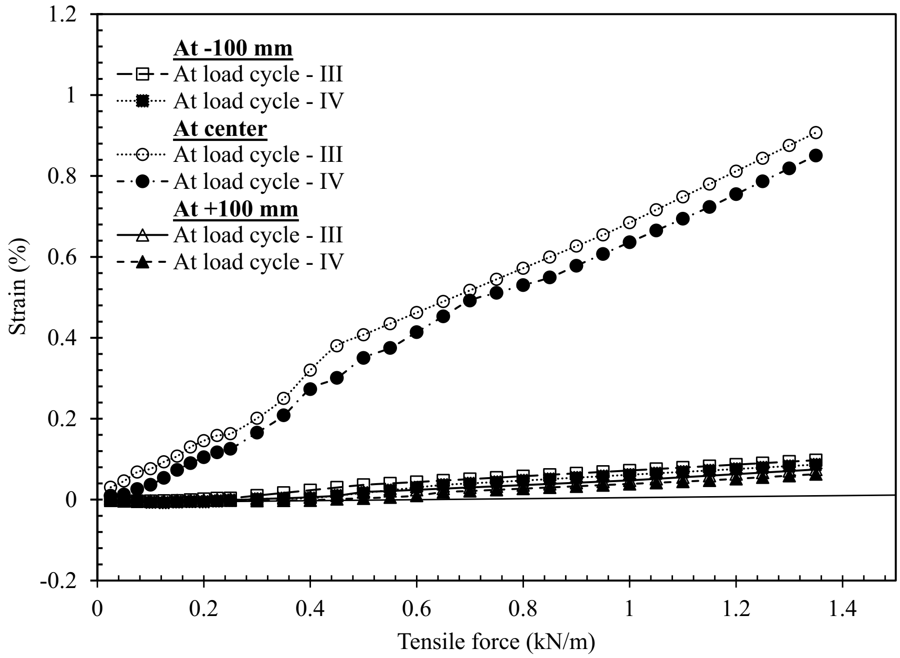

(i)

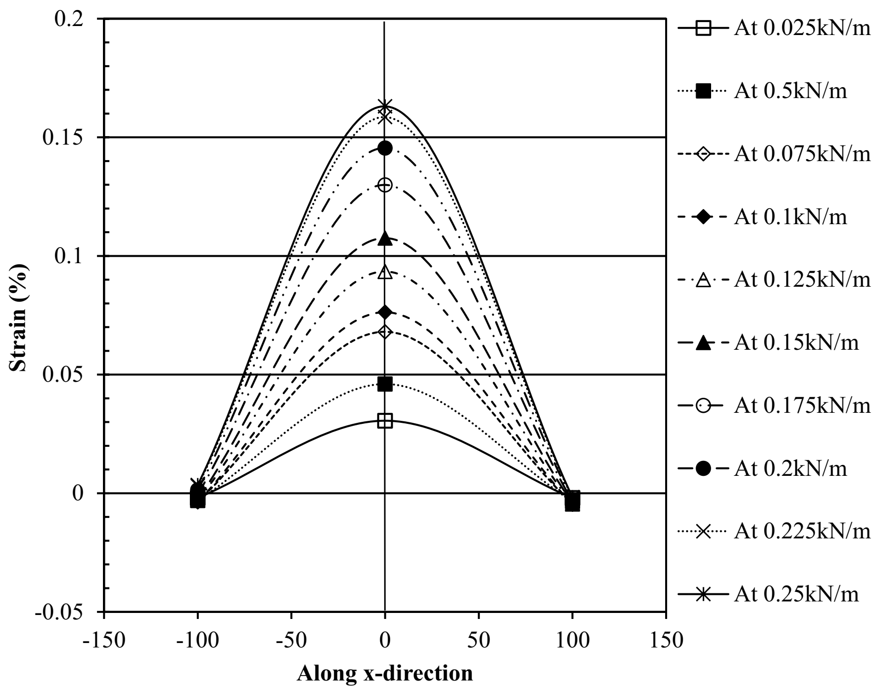

(ii)

(a)

Fig. 9 (continued)

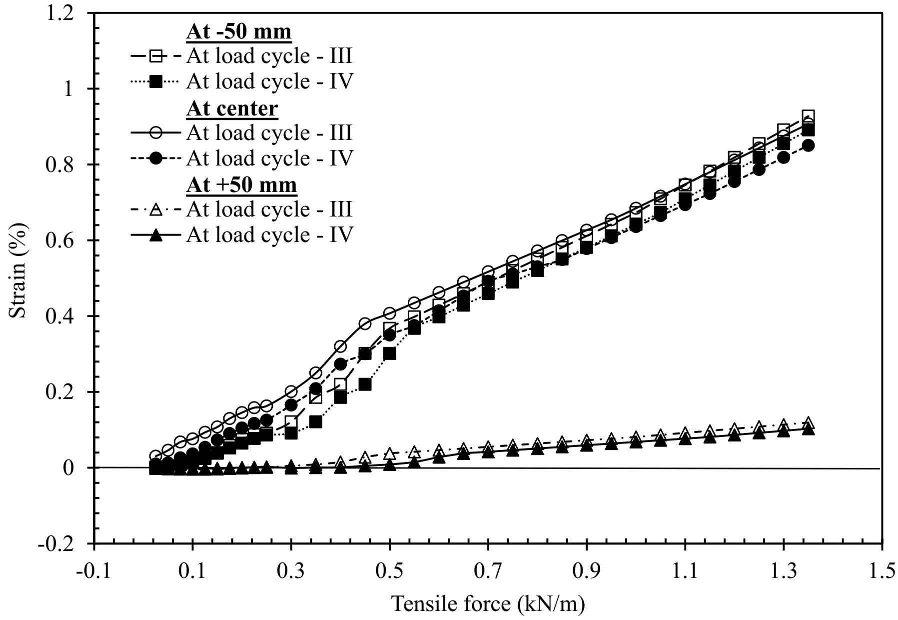

(i)

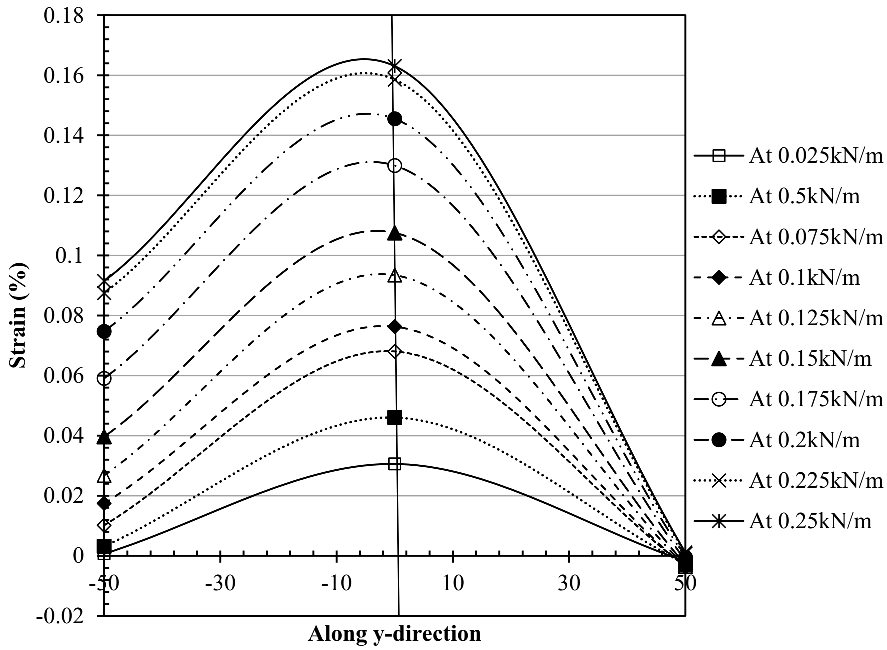

(ii)

(b)

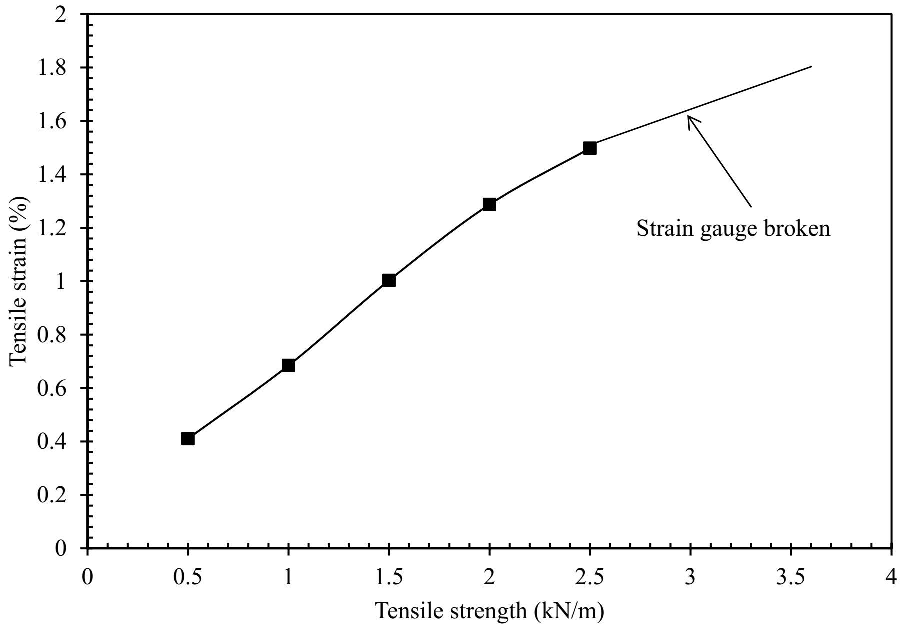

Fig. 10 Variation of mobilized strain distribution in wide-width tensile test jute geotextile sample during loading

Fig. 11 Testing of strain gauge prior placing into the test tank

jute geotextile reinforcement rather than the soil failure. It occurred due to at an optimum condition of *u/D* of 0.4, the overburden pressure of the sand bed on the reinforcement layer is sufficient to restrain the reinforcement layer, and thus resists the applied vertical loads until it fails by rupture. As a result, the bearing capacity or bearing capacity ratio (BCR) of reinforced sand bed increases up to the rupture failure of the jute geotextile reinforcement layer i.e., 18% as shown in Fig. 13, and thereafter, the BCR downwards in footing settlement ratio more than 18%.

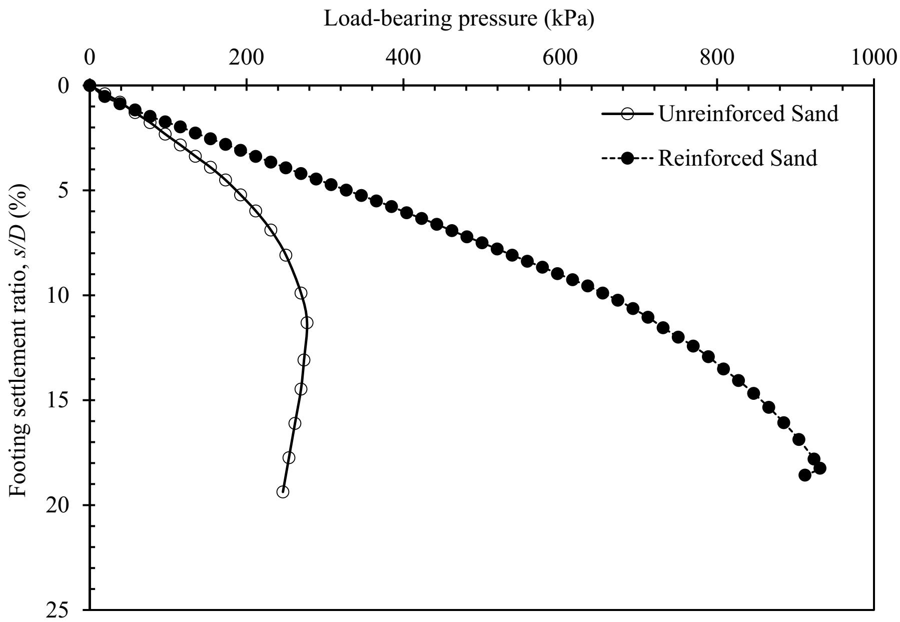

Fig. 12 Variation of load-settlement curves of unreinforced and muti layered reinforced sand bed

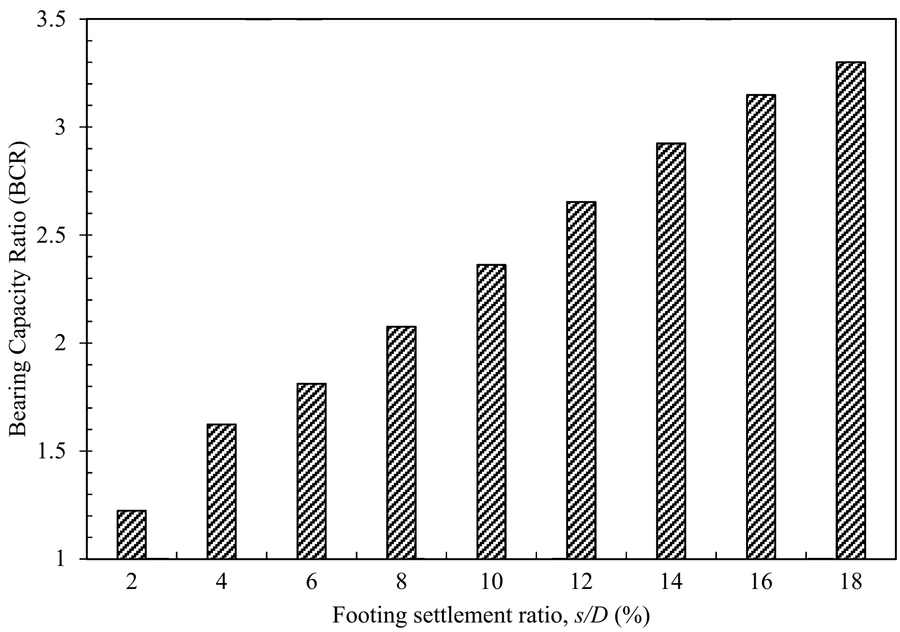

Fig. 13 Variation of bearing capacity ratio (BCR) of reinforced sand bed at different footing settlement ratios

Finally, Figs. 12 and 13 illustrates that the load-carrying capacity or BCR of the sand bed increases with increasing footing settlement ratios. Figure 14 shows the variation of mobilized tensile strains in the reinforcement layers along the vertical direction of the sand bed during loading or testing.

2.4 Criterion for Allowable Settlements

2.4.1 *According to Footing Settlement Criteria*

According IS: 1904–1986 (IS 1904), in the case of sands, the shallow isolated steel and concrete type of

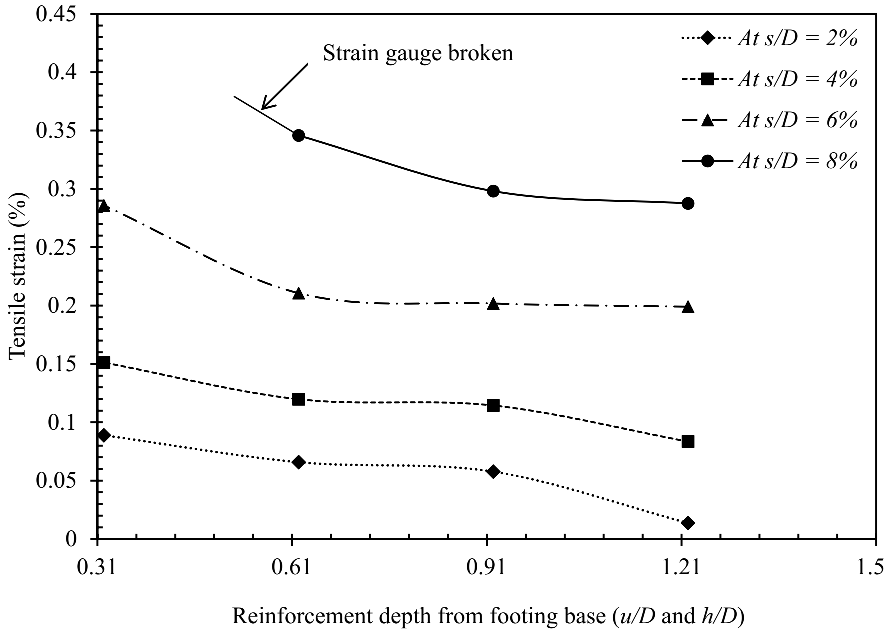

Fig. 14 A view of strain distribution along vertical direction of multilayered reinforced sand bed ($\frac{u}{D}=0.31$, $\frac{h}{D}=0.3$, $N=4$, $\frac{B_r}{D}=3.5$)

structural foundations should be allowed up to a certain settlement, i.e., 50 mm. As per scaling down factors presented in Table 1b, the present model footing having a diameter of 150 mm can be allowed up to a permissible settlement of 6.25 mm, and in terms of the settlement ratio (*s/D*) is 4.2%. From Fig. 13, the soil bearing capacity ratio corresponding footing settlement ratio (*s/D*) of 4% is 1.62.

2.5 According to Reinforcement Tensile Strain Criteria

As per Table 2, the scale-down tensile strain of model geotextile was 1%, which is matching with the prototype synthetic reinforcement tensile strain of 2%. From Fig. 5, the tensile load of the model jute geotextile corresponding to the tensile strain of 1% is 0.5 kN/m. The percentage of mobilized tensile strains developed in the reinforcement corresponding to the tensile load of 0.5 kN/m can be obtained from Fig. 10, i.e., 0.4%. From Fig. 14, it can be realized that the strain gauges placed at the top most reinforcement layers were failed or broken at the corresponding footing settlement ratio (*s/D*) of 8%. The variation of mobilized tensile strain data of the present study is consistent with strain distribution results in the literature (Abu-Farsakh et al. 2013; Saha Roy and Deb 2017). The corresponding mobilized tensile strain for footing settlement ratio (*s/D*) of 8% is around 0.35% to 0.4% (approximately). Therefore, based on the observed results presented in Fig. 14 and as per the allowable tensile strain of the reinforcements, the footing can be allowed up to the settlement ratio (*s/D*) of 8%, and the corresponding BCR value is 2.1 (Fig. 13).

Based on the above observations, the model footing can be allowed either according to the footing settlement condition or the allowable reinforcement tensile strain condition i.e., up to the footing settlement ratio (*s/D*) of 4% and 8%. However, as per the safety considerations, the footing should be allowed up to a certain value of the *s/D* ratio, which is lower in the above two criteria. Hence, according to the footing settlement condition and as per the obtained results, the footing can be allowed up to the footing settlement ratio (*s/D*) of 4% in order to understand the effect of reinforcement layers on the improvement of BCR. Further, the BCR value of sand bed corresponding *s/D* of 4% is 1.62 considered as maximum improvement with inclusion of reinforcement layers, even though the BCR is higher at a settlement less than the peak settlement of the unreinforced soil (Fragaszy and Lawton 1984; Yetimoglu et al. 1994; Saha Roy and Deb 2017; Huang and Tatsuoka 1990; Khing et al. 1993). For the same conditions, if the scale down factor (*N*) is considered to be 2, then the permissible settlement ratio (*s/D*) of the footing according to the criteria of footing settlement (i.e., 11% of *s/D*) and allowable reinforcement tensile strain (i.e., > 8% of *s/D*) may change as per the safety considerations. Therefore, the scaling factors play a major role in the determination of allowable footing settlements.

2.6 Limitations and Applicability

As explained in the previous sections, based on the strain gauge data presented in Fig. 10 and Fig. 14, the effect of reinforcement layers on the improvement of the load-carrying capacity of the footing can be predicted up to an allowable settlement ratio (*s/D*) of 8%. Notably, Figs. 10 and 14 present the strain gauge data of the geotextile corresponding to the conditions of unconfined and confined reinforcements. Further, in the case of confined conditions of the reinforcement, the mobilized tensile force or tensile modulus may be lower as compared to the unconfined conditions (Aria et al. 2019b). Moreover, the present laboratory model test studies were limited to 1*g* conditional sand beds and reinforced with single tensile stiffness of geotextile reinforcements. Also, the influence of particle size on the mobilized noticeable tensile strengths and stiffness of the reinforcements and imparting augmented bearing capacity is questionable.

2.7 Future Prospects

This section provides details about further needful studies that have to be carried out along with scarcity in the existing literature. Hence, this section paves the way for the future scope of research as described here follows:

1. Toyosawa et al. (2013) proposed a relationship for consideration of the particle size effect during model tests that were based on centrifuge model tests carried out on unreinforced sand beds. However, the influence of particle size in the case of reinforced soil beds is not yet clear and needs to be elucidated.
2. Confined wide-width tensile testing should be performed to understand the variation of mobilization of tensile strains in the reinforcements in comparison with the unconfined conditional reinforcement tensile strain results during loading.
3. Fig. 9a-b illustrate the higher mobilization of tensile strains at the central position of strain gauge irrespective of the direction and position of strain gauges on the reinforcements during loading. This might be due to the non-uniform distribution of stress along the length and width of the reinforcement layer during tensile loading. So, the present test results further reinforce the limitation in the assumption of uniform strain distribution throughout the test specimen during the tensile test (Chenari and Bathurst 2023a, 2023b; Kutay et al. 2006). However, in the present study, during the wide-width tensile testing, the failure or rupture occurs in the jute geotextile test sample exactly at the central portion without any further noticeable slippage. Hence, further model tests need to be performed using extensometers and digital image-based techniques for the proper evaluation of strain distribution in the reinforcements (Xia et al. 2021).
4. Furthermore, according to reinforcement tensile strain criteria, the allowable settlement of prototype footing corresponding to reinforcement tensile strain of 2% may be more than the model footing settlement, i.e., *s/D* of 8%, due to the difference in the values of tensile stiffness of model and prototype reinforcement material. This type of condition can occur even for the case of consideration of model reinforcement having lesser tensile stiffness (i.e., $1/N^2$ times) as compared with the prototype reinforcement for the same tensile strain (Buragadda and Thyagaraj 2019; Viswanadham and Konig 2004; Dhanya et al. 2019). Hence, for a complete understanding and application, the centrifuge model tests and numerical tests need to be performed with different tensile stiffness of reinforcements in order to predict the behavior of the real field conditional prototype reinforced soils.
5. The influence of reinforcement tensile stiffness on the footing load carrying capacity is need to be found out by considering the various range of tensile strengths and stiffness of reinforcements.
6. Aforementioned test studies could be performed using transparent box (such as Plexi-glass material) to capture the alteration of soil particle position and observation of failure mechanism and deformation pattern.

3 Conclusion

Based on the test results, the following conclusions were drawn:

(1) The present study was performed on a model jute geotextile reinforced sand under 1g condition by applying scaling laws to replicate the real behavior of the prototype in the field in real-time. A new approach was used in this present study for the consideration of model geotextile to simulate the real effect of prototype geotextile reinforcement material.
(2) According to footing settlement criterion, the model footing of the present study can be allowed up to a permissible settlement of 6.25 mm, and in terms of the settlement ratio *(s/D)* is 4.2%.
(3) According to the scale down factors of unconfined tensile strength test results, the tensile load of the model jute geotextile corresponding to the tensile strain of 1% is 0.5 kN/m. The percentage of mobilized tensile strains developed in the reinforcement corresponding to the tensile load of 0.5 kN/m can be obtained as 0.4%.
(4) According to bearing capacity test results, it can be realized that the strain gauges placed at the topmost reinforcement layers were failed or broken at the corresponding footing settlement ratio *(s/D)* of 8%. The corresponding mobilized tensile strain for footing settlement ratio *(s/D)* of 8% is around 0.35% to 0.4%.

Finally, it was concluded that the model footing can be allowed up to a certain settlement depending upon two criterions i.e., (i) footing settlement criteria and (ii) reinforcement tensile strain criteria, even though the effect of reinforcement on soil load-carrying capacity improvement is higher at the higher footing settlement ratios (*s/D*). The present study could be useful to understand the effect of reinforcement layers on the improvement of BCR up to a certain settlement ratio (*s/D*) of the footings. Notably, the present test observations are not only limited to the case of geotextile reinforced shallow foundations, but they will also be useful to understand the consideration of the effect of reinforcements in the case of geogrid and geocell reinforced foundations as well.

Acknowledgements The authors would like to acknowledge the formatting support extended by Mr. Muni Pavan Kompala, Ph.D. Research Scholar, National Institute of Technology Warangal, Warangal, Telangana State, INDIA.

Author contributions BV and ERO, conceptualized, designed, and carried out the experiments, analysed the results, and contributed to writing the original draft preparation.

Funding This research did not receive any specific grant from funding agencies in the public, commercial, or not-for-profit sectors.

Availability of data and material The data and materials presented in this paper are available.

Code availability Not applicable.

Declarations

Conflict of interest The author(s) declares no potential conflicts of interest concerning the research, authorship, and/or publication of this study.

References

ASTM D 6913–17 (2017) Standard test methods for particle-size distribution (gradation) of soils using sieve analysis. ASTM Int, West Conshohocken

ASTM D 4254–16 (2016) Standard test methods for minimum index density and unit weight of soils and calculation of relative density. ASTM Int, West Conshohocken

ASTM D 4595–17 (2017) Standard test method for tensile properties of geotextiles by the wide-width strip method. ASTM Int, West Conshohocken

ASTM D 5199–12 (2012) Standard test method for measuring the nominal thickness of geosynthetics. ASTM Int, West Conshohocken

ASTM D 5261–10 (2018) Standard test method for measuring mass per unit area of geotextiles. ASTM Int, West Conshohocken

ASTM D 6241–14 (2014) Standard test method for static puncture strength of geotextiles and geotextile-related products using a 50-mm Probe. ASTM Int, West Conshohocken

ASTM D 5321–17 (2017) Standard test method for determining the shear strength of soil-geosynthetic and geosynthetic-geosynthetic interfaces by direct shear. ASTM Int, West Conshohocken

Abid MS, Rathod D (2022) Bearing capacity of asphalt-coated jute textile reinforced sand. Geotech Geol Eng 40(7):3457–3475. https://doi.org/10.1007/s10706-022-02106-9

Abu-Farsakh M, Chen Q, Sharma R (2013) An experimental evaluation of the behavior of footings on geosynthetic-reinforced sand. Soils Found 53(2):335–348. https://doi.org/10.1016/j.sandf.2013.01.001

Adams MT, Collin JG (1997) Large model spread footing load tests on geosynthetic reinforced soil foundations. J

Geotech Geoenviron Eng 123(1):66–72. https://doi.org/10.1061/(ASCE)1090-0241(1997)123:1(66)
Akbar A, Bhat JA, Mir BA (2022) Laboratory study on pressure settlement behavior of shallow foundation on bitumen coated geogrid reinforced soil bed with varying percentage of prestress. Int J Pave Res Tech. https://doi.org/10.1007/s42947-021-00147-6
Akhil KS, Sankar N, Chandrakaran S (2019) Behaviour of model footing on bamboo mat-reinforced sand beds. Soils Found 59(5):1324–1335. https://doi.org/10.1016/j.sandf.2019.05.006
Aria S, Kumar Shukla S, Mohyeddin A (2019a) Numerical investigation of wraparound geotextile reinforcement technique for strengthening foundation soil. Int J Geomech 19(4):04019003. https://doi.org/10.1061/(ASCE)GM.1943-5622.0001361
Aria S, Shukla SK, Mohyeddin A (2019b) Tensile behaviour of geotextile reinforcement within the sandy soil supporting a strip footing. Geotech Lett 9(1):59–65. https://doi.org/10.1680/jgele.18.00169
Aria S, Shukla SK, Mohyeddin A (2021) Behaviour of sandy soil reinforced with geotextile having partially and fully wrapped ends. Proceed ICE Ground Improve 174(1):29–41. https://doi.org/10.1680/jgrim.18.00102
Basudhar PK, Saha S, Deb K (2007) Circular footings resting on geotextile-reinforced sand bed. Geotext Geomembr 25(6):377–384. https://doi.org/10.1016/j.geotexmem.2006.09.003
Binquet J, Lee KL (1975) Bearing capacity tests on reinforced earth slabs. J Geotech Eng Div 101:1241–1255. https://doi.org/10.1061/AJGEB6.0000219
Buragadda V, Thyagaraj T (2019) Bearing capacity of jute geotextile-reinforced sand bed. Int J Geosynth Ground Eng 5(4):1–14. https://doi.org/10.1007/s40891-019-0178-6
Chenari RJ, Bathurst RJ (2023a) Influence of geosynthetic stiffness on bearing capacity of strip footings seated on thin reinforced granular layers over undrained soft clay. Geotext Geomembr 51(1):43–55. https://doi.org/10.1016/j.geotexmem.2022.09.006
Chenari RJ, Bathurst RJ (2023b) Bearing capacity of strip footings seated on unreinforced and geosynthetic-reinforced granular layers over spatially variable soft clay deposits. J Geotech Geoenv Eng 149(6):04023034. https://doi.org/10.1061/JGGEFK.GTENG-10889
Chitrachedu RK, Kolathayar S (2020) Performance evaluation of coir geocells as soil retention system under dry and wet conditions. Geotech Geol Eng 38(6):6393–6406. https://doi.org/10.1007/s10706-020-01443-x
Cicek E, Guler E, Yetimoglu T (2015) Effect of reinforcement length for different geosynthetic reinforcements on strip footing on sand soil. Soils Found 55(4):661–677. https://doi.org/10.1016/j.sandf.2015.06.001
Cocjin M, Fujita T, Kusakabe O, Kitazume M (2013) Centrifuge Modeling of Embedment Effects on Eccentrically Loaded Shallow Foundation on Sand. In New Frontiers in Eng Geol Environ. https://doi.org/10.1007/978-3-642-31671-5_14
Dash SK, Rajagopal K, Krishnaswamy NR (2004) Performance of different geosynthetic reinforcement materials in sand foundations. Geosynth Int 11(1):35–42. https://doi.org/10.1680/gein.2004.11.1.35
Demir A, Laman M, Yildiz A, Ornek M (2013) Large scale field tests on geogrid-reinforced granular fill underlain by clay soil. Geotext Geomembr 38:1–15. https://doi.org/10.1016/j.geotexmem.2012.05.007
Demir A, Yildiz A, Laman M, Ornek M (2014) Experimental and numerical analyses of circular footing on geogrid-reinforced granular fill underlain by soft clay. Acta Geotech 9(4):711–723. https://doi.org/10.1007/s11440-013-0207-x
Dhanya JS, Boominathan A, Banerjee S (2019) Performance of geo-base isolation system with geogrid reinforcement. Int J Geomech 19(7):04019073. https://doi.org/10.1061/(ASCE)GM.1943-5622.0001469
Fayaz S, Shah MY (2023) Behavior of geosynthetic reinforced ring footings supported on multilayered soil Strata. Geotech Geol Eng. https://doi.org/10.1007/s10706-023-02544-z
Fragaszy RJ, Lawton E (1984) Bearing capacity of reinforced sand subgrades. J Geotech Eng Div 110(10):1500–1507. https://doi.org/10.1061/(ASCE)0733-9410(1984)110:10(1500)
Ghazavi M, Lavasan AA (2008) Interference effect of shallow foundations constructed on sand reinforced with geosynthetics. Geotext Geomembr 26(5):404–415. https://doi.org/10.1016/j.geotexmem.2008.02.003
Ghosh A, Ghosh A, Bera AK (2005) Bearing capacity of square footing on pond ash reinforced with jute-geotextile. Geotext Geomembr 23(2):144–173. https://doi.org/10.1016/j.geotexmem.2004.07.002
Guido VA, Chang DK, Sweeney MA (1986) Comparison of geogrid and geotextile reinforced earth slabs. Can Geotech J 23(1):435–440. https://doi.org/10.1139/t86-073
Guo X, Zhang H, Liu L (2020) Planar geosynthetic-reinforced soil foundations: a review. SN Appl Sci 2(12):1–18. https://doi.org/10.1007/s42452-020-03930-5
Hsieh C, Mao HL (2005) A bench-scale performance test for evaluation the geosynthetic reinforcement effects on granular base courses. In: GRI-18 Geosynthetics Research and Development in Progress. Geofrontiers, Austin, TX. https://doi.org/10.1061/40782(161)9
Huang CC, Tatsuoka F (1990) Bearing capacity of reinforced horizontal sandy ground. Geotext Geomembr 9:51–82. https://doi.org/10.1016/0266-1144(90)90005-W
IS 1888 (1982) Method of load test on soils. Bureau of Indian Standards, New Delhi, India.
IS 1904 (2017) Code of practice for design and construction of foundations in soils: General requirements. Bureau of Indian Standards Committee, New Delhi, India.
Kazi M, Shukla SK, Habibi D (2015) Behavior of embedded strip footing on sand bed reinforced with multilayer geotextile with wraparound ends. Int J Geotech Eng 9(5):437–452. https://doi.org/10.1179/1939787914Y.0000000085
Khing KH, Das BM, Puri VK, Cook EE, Yen SC (1993) The bearing capacity of a strip foundation on geogrid reinforced sand. Geotext Geomembr 12(4):351–361. https://doi.org/10.1016/0266-1144(93)90009-D

Kusakabe O (1993) Application of centrifuge modeling to foundation engineering. Foun Construction 11(1):1–10
Kusakabe O, Maeda Y, Ohuchi M (1992) Large-scale loading tests of shallow footings in pneumatic caisson. ASCE, J Geotech Eng 118(11):1681–1695
Kutay ME, Guler M, Aydilek AH (2006) Analysis of factors affecting strain distribution in geosynthetics. J Geotech Geoenviron Eng 132(1):1–11. https://doi.org/10.1061/(asce)1090-0241(2006)132:1(1)
Lal D, Sankar N, Chandrakaran S (2017) Effect of reinforcement form on the behaviour of coir geotextile reinforced sand beds. Soils Found 57(2):227–236. https://doi.org/10.1016/j.sandf.2016.12.001
Latha GM, Somwanshi A (2009a) Bearing capacity of square footings on geosynthetic reinforced sand. Geotext Geomembr 27(4):281–294. https://doi.org/10.1016/j.geotexmem.2009.02.001
Latha GM, Somwanshi A (2009b) Effect of reinforcement form on the bearing capacity of square footings on sand. Geotext Geomembr 27(6):409–422. https://doi.org/10.1016/j.geotexmem.2009.03.005
Liu F, Yang JJ, Ding YD (2007) Study on influence of footing shape and depth burial on bearing capacity by centrifugal tests. Architecture Tech 38(1):327–331
Mahmud MB, Zimmie TF (1997) Innovative and rapidly installed mechanically stabilized earth systems for highway embankments-model studies. Transp Res Rec 1582(1):1–7.
Okamura M, Takemura J, Ueno K (2004) Centrifugal model test – the technology and the applicability. 2. The similarity of centrifugal model test and the technology – advantage and disadvantage. Tsuchi-to-Kiso JGS 52(10):37–44
Ouria A, Mahmoudi A (2018) Laboratory and numerical modeling of strip footing on geotextile-reinforced sand with cement-treated interface. Geotext Geomembr 46(1):29–39. https://doi.org/10.1016/j.geotexmem.2017.09.003
Patra CR, Das BM, Atalar C (2005) Bearing capacity of embedded strip foundation on geogrid-reinforced sand. Geotext Geomembr 23(5):454–462. https://doi.org/10.1016/j.geotexmem.2005.02.001
Pinto MIM, Cousens TW (1999) Modelling a geotextile-reinforced, brick-faced soil retaining wall. Geosynth Int 6(5):417–447. https://doi.org/10.1680/gein.6.0159
Saha Roy S, Deb K (2017) Bearing capacity of rectangular footings on multilayer geosynthetic-reinforced granular fill over soft soil. Int J Geomech 17(9):04017069. https://doi.org/10.1061/(ASCE)GM.1943-5622.0000959
Sarsby RW (2007) Use of Limited Life Geotextiles'(LLGs) for basal reinforcement of embankments built on soft clay. Geotext Geomembr 25(4–5):302–310. https://doi.org/10.1016/j.geotexmem.2007.02.010
Shin EC, Das BM, Lee ES, Atalar C (2002) Bearing capacity of strip foundation on geogrid-reinforced sand. Geotech Geol Eng 20(2):169–180. https://doi.org/10.1023/A:1015059427487
Shukla S, Sivakugan N, Das B (2009) Fundamental concepts of soil reinforcement—an overview. Int J Geotech Eng 3(3):329–342. https://doi.org/10.3328/IJGE.2009.03.03.329-342
Skochdopole TR, Cassady L, Pihs D, Stevenson PE (2000) Comparative study of roller and wedge grips for tensile testing of high strength fabrics with laser extensometry: comparisons to LVDT and crosshead extension. In Grips, Clamps, Clamping Techniques, and Strain Measurement for Testing of Geosynthetics. ASTM Int. DOI: https://doi.org/10.1520/STP13472S
Tafreshi SM, Dawson AR (2010) Comparison of bearing capacity of a strip footing on sand with geocell and with planar forms of geotextile reinforcement. Geotext Geomembr 28(1):72–84. https://doi.org/10.1016/j.geotexmem.2009.09.003
Tafreshi SM, Sharifi P, Dawson AR (2016) Performance of circular footings on sand by use of multiple-geocell or-planar geotextile reinforcing layers. Soils Found 56(6):984–997. https://doi.org/10.1016/j.sandf.2016.11.004
Tatsuoka F, Goto S, Tanaka T, Tani K, Kimura Y (1997) Particle size effects on bearing capacity of footing on granular material. In: Proceedings of IS-NAGOYA, pp 133–138
Tavangar Y, Shooshpasha I (2016) Experimental and numerical study of bearing capacity and effect of specimen size on uniform sand with medium density, reinforced with nonwoven geotextile. Arab J Sci Eng 41(10):4127–4137. https://doi.org/10.1007/s13369-016-2101-y
Tavangar Y, Shooshpasha I (2020) Impacts of a nonwoven geotextile arrangement on load-bearing capacity of reinforced sand: a laboratory study. Innovat Infrastr Sol 5(1):1–9. https://doi.org/10.1007/s41062-019-0253-9
Toyosawa Y, Itoh K, Kikkawa N, Yang JJ, Liu F (2013) Influence of model footing diameter and embedded depth on particle size effect in centrifugal bearing capacity tests. Soils Found 53(2):349–356. https://doi.org/10.1016/j.sandf.2012.11.027
Viswanadham BVS, Konig D (2004) Studies on scaling and instrumentation of a geogrid. Geotext Geomembr 22(5):307–328. https://doi.org/10.1016/S0266-1144(03)00045-1
Wood DM (2004) Geotechnical modelling. Taylor & Francis, UK
Xia X, Zhang X, Mu C (2021) A multi-camera based photogrammetric method for three-dimensional full-field displacement measurements of geosynthetics during tensile test. Geotext Geomembr 49(5):192–1210. https://doi.org/10.1016/j.geotexmem.2021.03.012
Yetimoglu T, Wu JTH, Saglamer A (1994) Bearing capacity of rectangular footings on geogrid-reinforced sand. J Geotech Eng 120(12):2083–2099. https://doi.org/10.1061/(ASCE)0733-9410(1994)120:12(2083)

Publisher's Note Springer Nature remains neutral with regard to jurisdictional claims in published maps and institutional affiliations.